Available online at www.sciencedirect.com
ScienceDirect
Journal of Power Sources 168 (2007) 272–277
JOURNAL OF POWER SOURCES
www.elsevier.com/locate/jpowsour

Short communication

Synthesis and electrochemical characterization of $Li_{1.05}RE_xCr_yMn_{2-x-y}O_4$ spinel as cathode material for rechargeable Li-battery

Yanting Xie [a,b], Rudong Yang [a,*], Lan Yan, Lu Qi [b], Kehua Dai, Ping He

[a] *College of Chemistry and Chemical Engineering, Lanzhou University, Lanzhou 730000, PR China*
[b] *College of Chemistry and Molecular Engineering, Peking University, Beijing 100871, PR China*

Received 9 April 2006; received in revised form 24 September 2006; accepted 4 January 2007
Available online 17 January 2007

Abstract

The spinel phases of $Li_{1.05}RE_xCr_yMn_{2-x-y}O_4$ (RE = Sc, Ce, Pr, Tb; $0 \le x \le 0.05$; $0 \le y \le 0.1$) were prepared by a soft chemical method. The structural and electrochemical properties of $Li_{1.05}RE_xCr_yMn_{2-x-y}O_4$ were investigated by X-ray diffraction (XRD), Transmission electron microscopy (TEM) and charge–discharge experiments. Rare earth element-Sc and transition metal-Cr as co-substituents stabilize the spinel framework and improve charge–discharge performance. For $Li_{1.05}Sc_{0.01}Cr_{0.03}Mn_{1.96}O_4$, the capacity of the cell maintained 95% of the initial capacity at the 80th cycle. The rare earth elements of the variable valent metals such as $Ce^{3+/4+}$, $Pr^{3+/4+}$, $Tb^{3+/4+}$ with transition metal Cr^{3+} as co-substituent do not stable framework of spinel or improve the cycling performance. Cyclic voltammetry (CV) were measured to provide clues for the improved cycling performance of cathode electrodes.

Keywords: Secondary Li-ion battery; Co-doped lithium manganese spinels; Cyclic voltammetry

1. Introduction

With the worldwide price markup of nickel and cobalt, the lithium manganese spinel has become an attractive cathodic material for lithium-ion rechargeable battery due to its low cost, less toxicity to the environments and relatively high energy density [1–3]. More recently, we had reported that the composition of $Li_{1.05}Sc_{0.01}Mn_{1.99}O_4$ among various $Li_{1.05}RE_{0.01}Mn_{1.99}O_4$ (RE = Sc, Y, La, Gd) samples showed good cycling behavior [4]. The partial substitution of the manganese ion in the 16d octahedral site enhances the framework of $Li_{1.05}Sc_{0.01}Mn_{1.99}O_4$, and improved the cycling performance. Similarly, Cr^{3+} as a substituent has been investigated by a number of groups [5–12]. Guohua et al. [13] have suggested that the improvement of the stability is due to stronger M–O bonding of the MO_6 octahedron of partially substituted $LiMn_{2-y}M_yO_4$ (M = Co, Cr, Ni) in comparison with that of Mn–O of the parent $LiMn_2O_4$ spinel. Chromium incorporation has been shown to stabilize the spinel structure by enhancing Mn–O covalency, removing manganese from the tetrahedral sites, and reducing the Jahn–Teller effect [10].

In this paper, a series of spinel phases of $Li_{1.05}RE_xCr_yMn_{2-x-y}O_4$ with variable valent metals such as $Ce^{3+/4+}$, $Pr^{3+/4+}$, $Tb^{3+/4+}$ or stable valent metal of that (Sc^{3+}) and transition metal Cr as co-substituents were prepared and their electrochemical properties were investigated. We found a better cycling performance for the rare earth metal with transition metal co-substituent spinel $Li_{1.05}Sc_xCr_yMn_{2-x-y}O_4$ compared to that of single one of them doped $Li_{1.05}Mn_2O_4$, which may be contributed by the co-substituting cations leading to a more stable spinel framework with good capacity retention rate.

2. Experiments

2.1. Materials and sample preparation

The starting metal salts [$LiNO_3$ (AR), Sc_2O_3 (>99.99%), $Mn(OAc)_2{\cdot}4H_2O$ (AR) and $Cr(NO_3)_3{\cdot}xH_2O$ (AR)] were used as received. An aqueous solution of $LiNO_3$ was prepared by dissolving in distilled water and the metal content was determined by means of Li_2SO_4 gravimetry. Solution of $Sc(NO_3)_3$ was prepared by dissolving Sc_2O_3 in dilute HNO_3

* Corresponding author. Tel.: +86 9318912513; fax: +86 9318912582.
E-mail address: xieyanting03@st.lzu.edu.cn (R. Yang).

0378-7753/$ – see front matter © 2007 Published by Elsevier B.V.
doi:10.1016/j.jpowsour.2007.01.019

and titrated with standard EDTA solution. The same way for preparing the solution of $Ce(NO_3)_3$ (0.29 mol L^{-1}), $Pr(NO_3)_3$ (0.09683 mol L^{-1}) and $Tb(NO_3)_3$ (0.1730 mol L^{-1}). In the case of preparing $Li_{1.05}Sc_{0.01}Cr_{0.01}Mn_{1.98}O_4$, the procedure is as follow: $Mn(OAc)_2{\cdot}4H_2O$ (Mn^{2+} is 15.84 mmol) was mixed with a solution of 8.4 mmol $LiNO_3$, 0.08 mmol $Sc(NO)_3$ and 0.08 mmol $Cr(NO_3)_3$. The resulting mixture was stirred at 70–80 °C vigorously for 10 min to give a clear mixture, to which ethanol (2 mL) was added and the mixture was evaporated gradually with constant stirring.

$Li_{1.05}RE_{0.01}Cr_{0.01}Mn_{1.98}O_4$ (RE = Sc, Ce, Pr, Tb) and Sc–Cr co-doped $Li_{1.05}Sc_xCr_yMn_{2-x-y}O_4$ ($0.01 \le x \le 0.05$, $0 \le y \le 0.1$) samples were prepared in starting molar ratio Li:RE:Cr:Mn = 1.05:x:y:$2-x-y$ by the above-mentioned method. The annealing experiments of products were done in a muffle furnace. The above-prepared precursor powders were placed into a alumina crucible, which is wide open to the air. The powder was preheated at 400 °C for 10 h, cooled to room temperature gradually in the furnace, and then ground. This material was annealed at temperature 750 °C for 24 h, cooled to room temperature gradually in the furnace. The fine dark powders were characterized and subjected to electrochemical property analysis.

2.2. Physical measurements and electrochemical studies

X-ray diffraction (XRD) analysis was conducted on a Rigaku D/Max-2400 diffractor using Cu Kα radiation (λ = 1.54056 Å). The diffraction patterns were taken at room temperature in the 2θ range of $5^\circ \le \theta \le 80^\circ$. Lattice parameters measured at MEAS_MODE = FT, SPEED_DIM is sec./step (FT), STEP = 0.02, KV = 40, mA = 150. The morphology and the grain sizes of the samples were obtained on JEM-1200EX Transmission electron microscopy (TEM).

Electrochemical measurements were performed using test cells, made of Teflon with the powdered synthetic spinels as cathodic material. Li metal as the anode electrode, Celgard 2400 membrane was used as the separator between cathode and anode. The typical composite cathode consisted of the mixture of spinel sample powders, acetylene black and poly-vinylidene fluoride (PVDF) dissolved in 1-methyl-2-pyrolidinone (NMP) in the 80:15:5 weight ratio. The above mixture was spread on electrodes of 16 mm diameter aluminium disk, and subsequently heated to 110 °C for 20 h. The electrolyte was prepared by dissolving 1.0 M $LiPF_6$ in ethylene carbonate (EC) and dimethyl carbonate (DMC) (1:1, v/v). The cells were fabricated hermetically. All cells were assembled in a dry glove box under nitrogen.

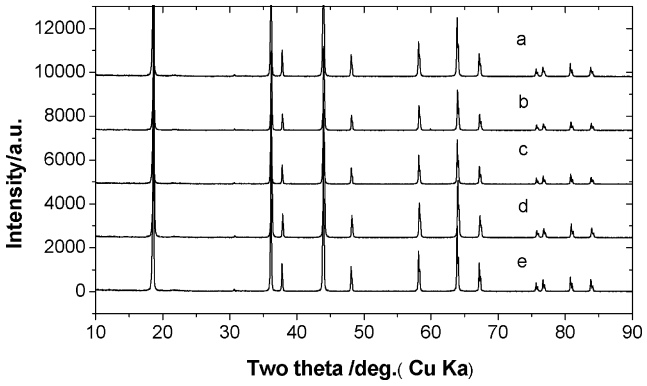

Fig. 1. Powder X-ray diffraction patterns of various $Li_{1.05}Sc_{0.01}Cr_yMn_{1.99-y}O_4$ (y = 0.00, 0.01, 0.03, 0.05, 0.07, and 0.1) spinel samples; (a) y = 0.00; (b) y = 0.01; (c) y = 0.03; (d) y = 0.05; (e) y = 0.07; (f) y = 0.10.

Three-electrode electrochemical cells were employed for electrochemical measurements using lithium foils as the counter and reference electrodes. Cyclic voltammograms were measured on a CHI660B electrochemistry workstation (Chen Hua, Shanghai, China) with a scan rate of 0.05 mV s^{-1} between 3.0 and 4.8 V (versus Li/Li^+). Charge and discharge performance of the cell was performed at a current density of 40 mA g^{-1} using the Land CT2001A (Wuhan, China) cycle testing system, with cut-off voltage of 3.0–4.4 V (versus Li/Li^+).

3. Results and discussion

3.1. Structural analysis and morphology of samples

The powder X-ray diffraction (XRD) patterns of the $Li_{1.05}Sc_xCr_yMn_{2-x-y}O_4$ ($0.01 \le x \le 0.02$, $0 \le y \le 0.1$) are shown in Fig. 1. All the samples within solid-solution limit were identified as a single phase of cubic spinel structure with a space group Fd_{3m} in which Li^+ occupies the tetrahedral (8a) sites. The Mn^{3+} and Mn^{4+} ions as well as Sc^{3+}, Cr^{3+}as in $LiMn_2O_4$ structure, occupy the octahedral (16d) sites, and the O^{2-} ion occupies the octahedral (32e) sites. Co-doping did not change the spinel structures since no impurity peaks were observed in the XRD patterns. The Powder X-ray diffraction patterns of $Li_{1.05}RE_{0.01}Cr_{0.01}Mn_{1.98}O_4$ ((a) RE = Ce, (b) RE = Pr, and (c) RE = Tb) is shown in Fig. 2. It is obvious that some other phases which corresponds to CeO_2 (JCPDS: 75-0120), Pr_6O_{11} (JCPDS: 41-1219), and $TbLiO_2$ (JCPDS: 73-0144) appeared in the Re (Ce, Pr or Tb) co-doped spinels, respectively.

The cubic lattice parameters of $Li_{1.05}Sc_xCr_yMn_{2-x-y}O_4$ are given in Table 1. Spinel $Li_{1.05}Mn_2O_4$ with typical spinels

Table 1
Lattice parameters of $Li_{1.05}Sc_xCr_yMn_{2-x-y}O_4$ (x = 0.00 and 0.01; 0.03 y = 0.00, 0.01, 0.03, 0.05, and 0.10) samples

x	0.00	0.01	0.03	0.01	0.01	0.01	0.01	0.01
y	0.00	0.00	0.00	0.01	0.03	0.05	0.07	0.10
Standard	0.0002	0.0002	0.0002	0.0002	0.0002	0.0002	0.0002	0.0002
A (Å)	8.2396	8.2429	8.2435	8.2371	8.2346	8.2306	8.2308	8.2331
Unit volume (Å^3)				558.89	558.37	557.57	557.60	558.08

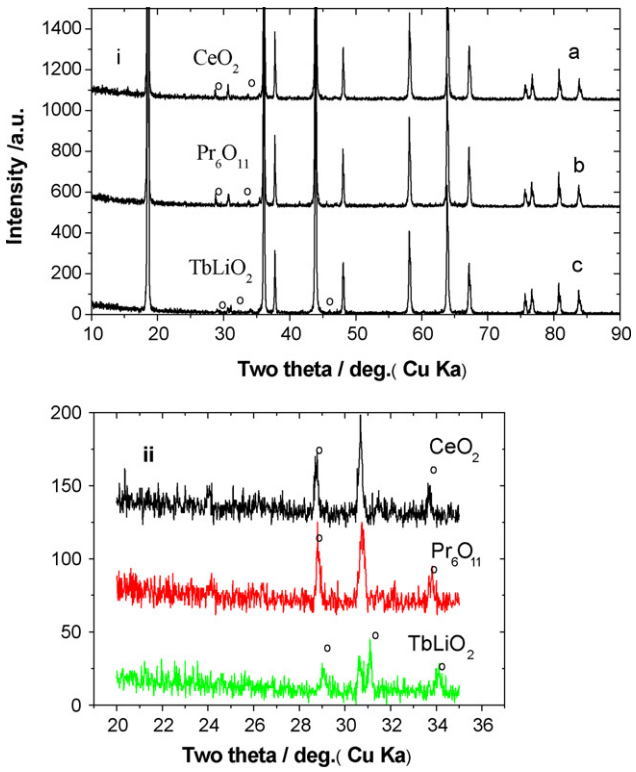

Fig. 2. (i) Powder X-ray diffraction patterns of $Li_{1.05}RE_{0.01}Cr_{0.01}Mn_{1.98}O_4$ ((a) RE = Ce (b) RE = Pr and (c) RE = Tb) and (ii) magnified of (i) from 20 to 35°.

characteristic peaks, which the lattice parameter is 8.2396 Å, but for Sc substituted spinel products, we had reported that solid solutions were formed, and the lattice parameters increased with the Sc contents from 0 to 0.03.

It is reported that Sc^{3+} ion with large ionic radius (0.745 Å) than Mn^{3+} (0.645 Å) [4]. Wang et al. reported that the lattice parameters of $LiCr_xMn_{2-x}O_4$ decreased with increase of the dopant Cr content [14]. It is commonly accepted that the substitution of Cr^{3+} has a smaller ion radius (0.615 Å) for Mn^{3+} (0.645 Å) leads to a lattice cell contraction. In our co-subsitituted $Li_{1.05}Sc_xCr_yMn_{2-x}O_4$ sample, as compared with $Li_{1.05}Mn_2O_4$, the lattice parameters and unit volume decrease with the amount of Cr ($0 \le y \le 0.05$) increasing when the x is 0.01. However, the lattice parameters and unit volume have a tendency to increase with increasing the further substituted Cr content ($0.05 \le y \le 0.1$). It is shown that the lattice parameters of $Li_{1.05}Sc_xCr_yMn_{2-x-y}O_4$ increase ($0.05 \le y \le 0.1$) as well as without any impure phases appeared. With the homogeneous distribution of Sc ions and Cr ion in $Li_{1.05}Mn_2O_4$ spinel structure, the co-dopant effect is expected to be maximized to decrease the capacity fade on cycling.

Particle morphology was examined using transmission electron microscopy (Fig. 3), $Li_{1.05}Sc_{0.01}Cr_{0.01}Mn_{1.98}O_4$ and $Li_{1.05}Sc_{0.01}Cr_{0.03}Mn_{1.96}O_4$ exhibited homogeneous particle distribution and small particles with similar particle shape. The particle sizes of these samples synthesized in our method ranged from 100 to 300 nm in nanometer scale with a wide distribution. The narrow particle size distribution of as prepared samples is important for good electrochemical properties.

3.2. Electrochemical property

The lithium self-assembled cells were cycled galvanostatically in the voltage range of 3.0–4.4 V. Fig. 4 shows the typical charge/discharge curves of $Li//Li_{1.05}Sc_{0.01}Cr_{0.01}Mn_{1.98}O_4$ and $Li//Li_{1.05}Sc_{0.01}Cr_{0.03}Mn_{1.96}O_4$ cells at a constant charge–discharge rate of C/3. For $Li_{1.05}Sc_{0.01}Cr_{0.03}Mn_{1.96}O_4$ electrode, two steps for lithium intercalating and deintercalating into the material of charge and discharge were obviously observed, and after 48 charge–discharge cycles, which is still two distinctive voltage plateaus with a pure and good spinel structure, but for $Li_{1.05}Sc_{0.01}Cr_{0.01}Mn_{1.98}O_4$ electrode, after 30 cycles, the two voltage plateaus are not very clear, The worst is $Li_{1.05}Re_{0.01}Cr_{0.01}Mn_{1.98}O_4$ (Re = Pr, Tb) electrodes, which is already not two plateaus at the first discharge. Compared with $LiMn_2O_4$ spinel, co-doped sample relatively blurry due to a small amount of Sc–Cr co-substitution, increasing the repulsive interaction between lithium positive–positive ions in the oxide lattice, the result is consistent with the reports of Myung et al. [15].

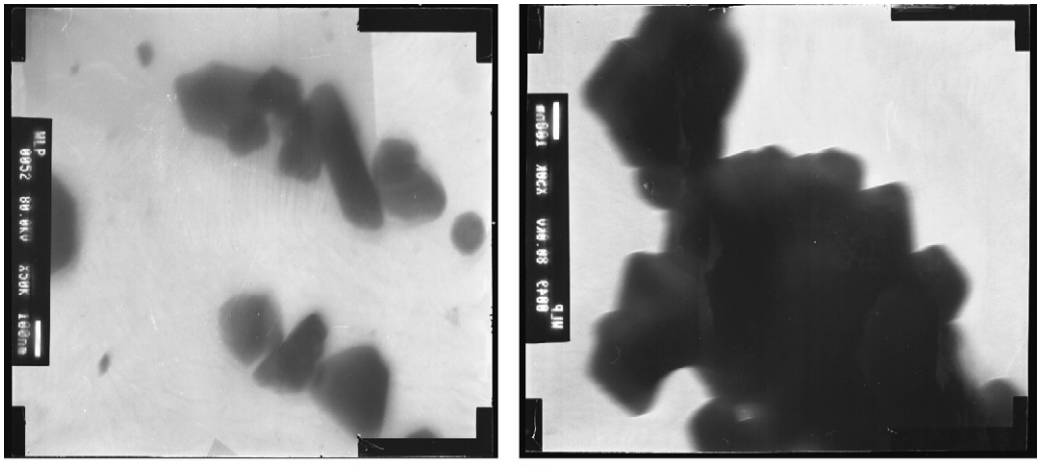

(a) (b)

Fig. 3. TEM images of the products (a) $Li_{1.05}Sc_{0.01}Cr_{0.01}Mn_{1.98}O_4$ (left); (b) $Li_{1.05}Sc_{0.01}Cr_{0.03}Mn_{1.96}O_4$ (right).

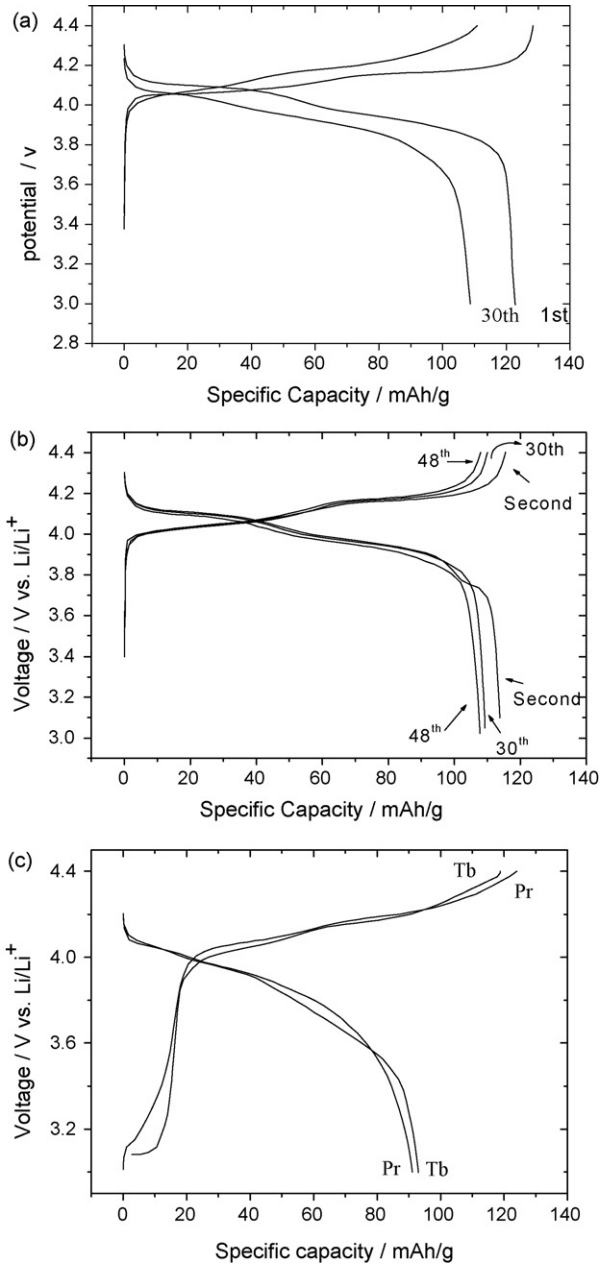

Fig. 4. Charge–discharge curves of (a) $Li_{1.05}Sc_{0.01}Cr_{0.01}Mn_{1.98}O_4$ and (b) $Li_{1.05}Sc_{0.01}Cr_{0.03}Mn_{1.96}O_4$ compared with (c) $Li_{1.05}RE_{0.01}Cr_{0.01}Mn_{1.98}O_4$ (Pr, Tb) samples with the first charge–discharge cycle.

As shown in Fig. 5, the cycle performance of the Sc–Cr co-doped spinels materials Li//$Li_{1.05}$ $RE_{0.01}Cr_{0.01}Mn_{1.98}O_4$ (RE = Sc, Ce, Pr, Tb) displayed good cyclability in terms of discharge capacity and cycle-life. Better cyclability is probably due to the substitution of some Mn–O linkages in the spinel by

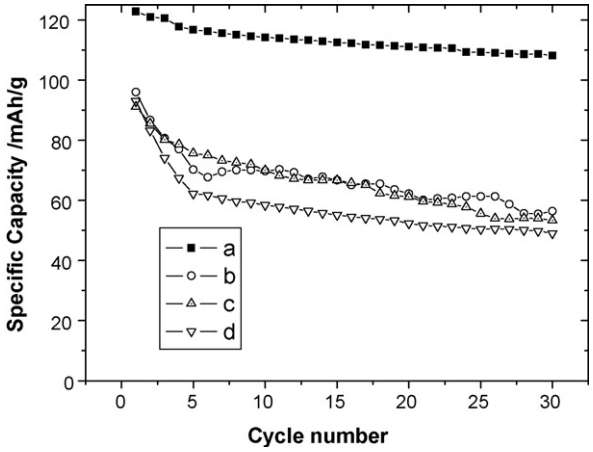

Fig. 5. Cycle performance of the Li//$Li_{1.05}$ $RE_{0.01}Cr_{0.01}Mn_{1.98}O_4$ cells (a) RE = Sc; (b) RE = Ce; (c) RE = Pr; (d) RE = Tb.

Sc–O and Cr–O simultaneously. The co-doped Cr^{3+} and invariable valence Sc^{3+}cations enhance the stability of the octahedral sites in the spinel skeleton structure. But for the variable valence rare earth metal including $Ce^{3+/4+}$, $Pr^{3+/4+}$, $Tb^{3+/4+}$ with Cr^{3+} co-substituted did not have a good stability and their specific capacities still quickly decayed. It is relative with the rare earth of Ce^{3+} (1.01 Å), Pr^{3+} (0.99 Å) or Tb^{3+} (0.923 Å) that are much larger ionic radius than Sc^{3+} (0.745 Å) in the co-doped samples. Maybe which valence states are not stable at octahedral site in spinels framework. The initial discharge capacity of $Li_{1.05}Ce_{0.01}Cr_{0.01}Mn_{1.98}O_4$ is only 96.0 mAh g^{-1}, after 30th cycles, it quickly decade to about 56.0 mAh g^{-1}, similar results with $Li_{1.05}Pr_{0.01}Cr_{0.01}Mn_{1.98}O_4$ and $Li_{1.05}Tb_{0.01}Cr_{0.01}Mn_{1.98}O_4$ samples. This may account for their poor cycling results which may be caused by the relatively large radius difference between the Re (Ce, Pr or Tb) and Mn^{3+} from Table 2.

Fig. 6 shows the discharge properties of $Li_{1.05}Mn_2O_4$ and $Li_{1.05}Sc_{0.02}Mn_{1.98}O_4$ for comparing with Sc–Cr co-doped $Li_{1.05}Sc_{0.01}Cr_{0.01}Mn_{1.98}O_4$. Obviously, good cyclability for co-doped sample than single one of Sc^{3+} doped in spinel sample. For $Li_{1.05}Sc_xCr_yMn_{2-x-y}O_4$, Sc^{3+} and Cr^{3+}co-replaced the place occupied originally by Mn^{3+} and the amount of Mn^{3+} in spinel was reduced by the increasing amount of Sc^{3+} or Cr^{3+}. As well as the amount of removable Li^+ is determined by the amount of Mn^{3+} [16], which is consistent with the results shown in Fig. 7. When Sc and Cr content increases simultaneously, the discharge capacity not well (Fig. 7). The initial discharge capacities of these powders decrease with increasing co-substitution content because of a decrease in the amount of extractable Li ion in the spinel phases. Inversely, if fixed Sc content, only as Cr content increases, Fig. 8 shows that the discharge capacity reten-

Table 2
Radius of various doping ions in $Li_{1.05}M_xRE_yMn_{2-x-y}O_4$ spinel samples

	Mn^{3+}	Cr^{3+}	Sc^{3+}	Ce^{4+}	Tb^{3+}	Pr^{3+}
$r(RE^{3+})/(CN=6)$ Å	0.645	0.615	0.745	0.87	0.923	0.99
$\|\Delta\| = r(Cr^{3+}, RE^{3+}) - r(Mn^{3+})$	–	0.03	0.1	0.34	0.278	0.345

Li^+: 0.76 (CN = 6)/0.59 Å (CN = 4).

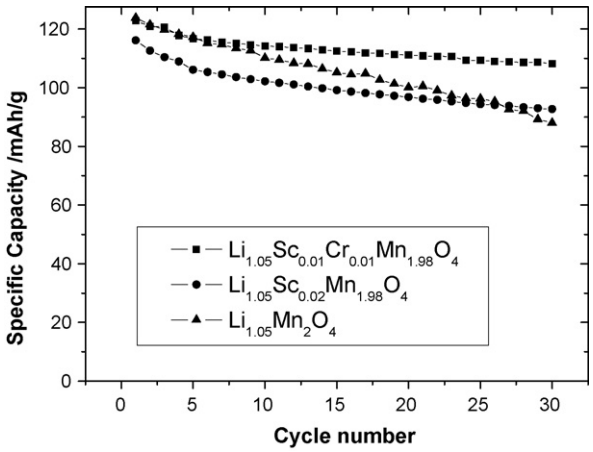

Fig. 6. Discharge properties of Li//$Li_{1.05}Sc_xCr_yMn_{2-x-y}O_4$ cells: (a) $x=y=0.01$; (b) $x=0.02$ and $y=0.00$; (c) $x=0.00$, $y=0.00$; at a current density of 40 mAh g^{-1}.

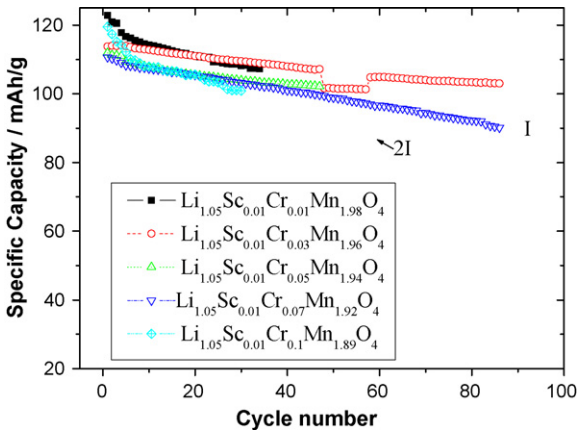

Fig. 8. Discharge capacities vs. cycle number of the Li// $Li_{1.05}Sc_{0.01}Cr_yMn_{1.99-y}O_4$ ($y=0.00$, 0.01, 0.03, 0.05, 0.07 and 0.1) cells, at current density of 40 mAh g^{-1}.

tion rate after 30 cycles is 88% for $Li_{1.05}Sc_{0.01}Cr_{0.01}Mn_{1.98}O_4$, 96% for $Li_{1.05}Sc_{0.01}Cr_{0.03}Mn_{1.96}O_4$, 93% for $Li_{1.05}Sc_{0.01}Cr_{0.05}Mn_{1.94}O_4$, 92.6% for $Li_{1.05}Sc_{0.01}Cr_{0.07}Mn_{1.92}O_4$ and 84% for $Li_{1.05}Sc_{0.01}Cr_{0.1}Mn_{1.89}O_4$. The strength of Sc–O bonding (-1819.36 kJ mol^{-1}) or Cr–O (-1058 kJ mol^{-1}) is higher than Mn–O bonding (-881.13 kJ mol^{-1}) on the basis of standard Gibbs energies of the formation of the both oxides at 298 K [17]. Therefore, considering the initial specific discharge capacity and the capacity retention rate, sample $Li_{1.05}Sc_{0.01}Cr_{0.03}Mn_{1.96}O_4$ exhibited good cycling performance, with initial discharge capacity of 113.8 mAh g^{-1} and capacity retention rate of 91% after 80 cycles. For $Li_{1.05}Sc_{0.01}Cr_{0.01}Mn_{1.98}O_4$ electrodes, after thirty cycles, the discharge capacities were still about 108 mAh g^{-1} in our study.

The cyclic voltammograms (CVs) were performed for the co-doped systems between 3.00 and 4.8 V at a scanning rate 0.05 mV s^{-1} show two regions of electrochemical activity. Fig. 9 compares the cyclic voltammetric behavior of a fresh Li//$Li_{1.05}Sc_{0.01}Cr_{0.03}Mn_{1.96}O_4$ cell with that of after 30 consecutive galvanostatic charge–discharge cycles (at C/3 rate) in the same potential range. The anodic and cathodic peaks observed in the CV of the fresh electrode exhibit reversible oxidation and reduction reactions. The split of the redox peaks into two couples indicates that the electrochemical reactions of the insertion and extraction of Li ion proceed in two stages [18]. Even after 30 number charge–discharge cycles, it is hardly any shift in the potential of the anodic peaks in the cyclic voltammograms for Li//$Li_{1.05}Sc_{0.01}Cr_{0.03}Mn_{1.98}O_4$ cell. It can be considered that the increased capacity and cycling property are due to the excellent stability of crystal structure caused by Sc–Cr incorporation.

CV graphs of Li//$Li_{1.05}Sc_{0.01}Cr_{0.01}Mn_{1.98}O_4$ with Fresh and 30th charge–discharge cycles and compared with fresh Li//$Li_{1.05}Sc_{0.01}Ce_{0.01}Mn_{1.98}O_4$ cells were shown in Fig. 10 (a and b, respectively). From CVs (i), two couples of oxidation and reduction peaks can be easily identified in fresh Li//$Li_{1.05}Sc_{0.01}Cr_{0.01}Mn_{1.98}O_4$ cell. With 30th cycling, the CV peaks became much less sharp and the peak separation became blurry than that of the fresh electrode. Moreover, the peaks current for the cycled electrode is much lower than that for the fresh ones. It means that further cycling leads

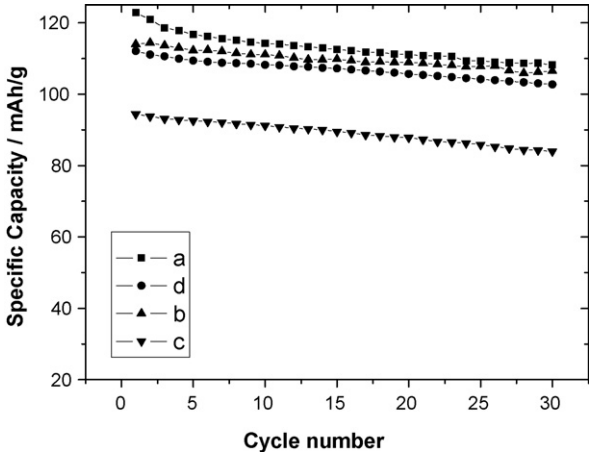

Fig. 7. Discharge properties of Li//$Li_{1.05}Sc_{x/2}Cr_{x/2}Mn_{2-x}O_4$ cells: (a) $x=0.02$; (b) $x=0.06$; (c) $x=0.1$; (d) $Li_{1.05}$ $Sc_{0.03}Cr_{0.01}Mn_{2-x}O_4$.

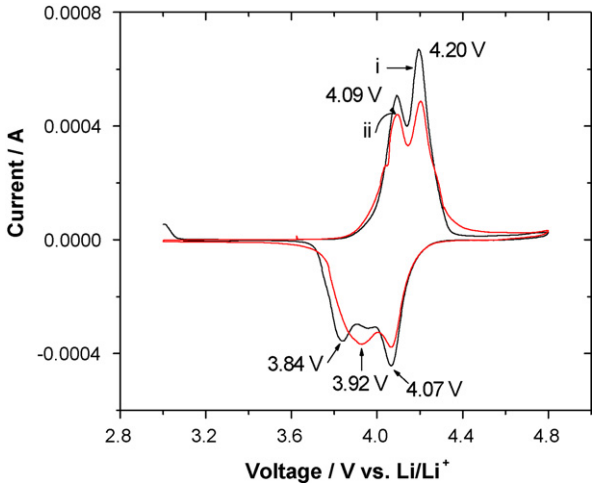

Fig. 9. Cyclic voltammograms graphs of Li//$Li_{1.05}Sc_{0.01}Cr_{0.03}Mn_{1.96}O_4$ cells ((i) fresh; (ii) after 30 charge–discharge cycles) with scan rate of 0.05 mV s^{-1}.

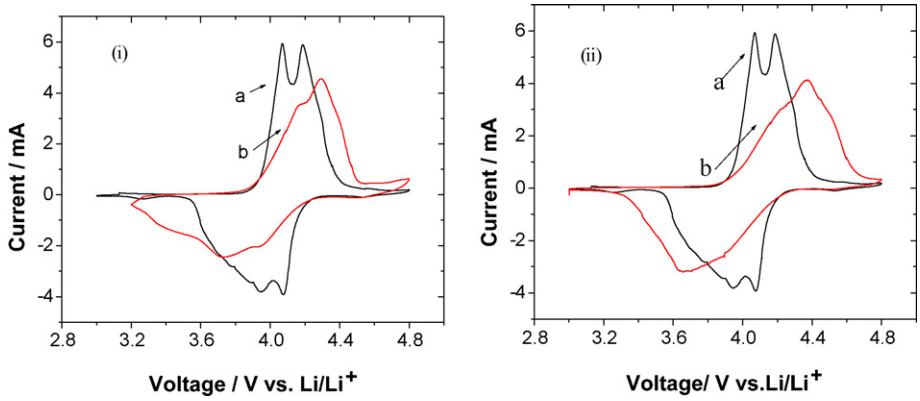

Fig. 10. Cyclic voltammograms graphs of (i) Li//$Li_{1.05}Sc_{0.01}Cr_{0.01}Mn_{1.98}O_4$ cell (a) fresh and (b) 30 charge–discharge cycles; (ii) fresh Li//$Li_{1.05}Sc_{0.01}Cr_{0.01}Mn_{1.98}O_4$ cell (a) and fresh Li//$Li_{1.05}Sc_{0.01}Ce_{0.01}Mn_{1.98}O_4$ cell (b) with scan rate of 0.05 mV s^{-1}.

to a pronounced capacity fading of the electrode. For fresh Li//$Li_{1.05}Sc_{0.01}Ce_{0.01}Mn_{1.98}O_4$ cell in CVs ii, it is suggest that two steps process or electrochemical characteristics for variable RE^{3+} (Ce, Pr Tb) as co-adopants materials cannot be found. They must essentially represent any differences between doping with rare earth metal cation in which the valance is variable or unvariable. Fig. 10(i) and (ii) illustrate the effect of different doped rare earth metals. This might be explained that the Ce–Cr co-dopants effect does significantly disturb the $LiMn_2O_4$ spinel structure. As a result, during intercalation–deintercalation of Li^+ only in Sc–Cr co-substituted $Li_{1.05}Sc_xCr_yMn_{2-x-y}O_4$, the kinetic characteristics of the electrode are also improved.

4. Conclusions

Simultaneous substitution of Cr and Sc or Ce, Pr, Tb for Mn in the $LiMn_2O_4$ spinel phase was attempted with the aim of developing a stable spinel framework with good capacity retention. Cathode materials of the Sc–Cr co-doped $Li_{1.05}Sc_xCr_yMn_{2-x-y}O_4$ spinels demonstrated substantially improved capacity retention on cycling than $Li_{1.05}Sc_xMn_{2-x}O_4$ or $Li_{1.05}Cr_yMn_{2-y}O_4$ for lithium-ion batteries. X-ray diffraction studies showed that Sc–Cr doped spinel formed phase-pure compounds in the compositional range studied. However, both co-doping of Sc and Cr led to decrease in the lattice parameters ($y \leq 0.05$). Cyclic voltammograms showed that two these co-doped spinel phases were less stable electrochemically for Ce–Cr co-doped spinel phase and more stable electrochemically for $Li_{1.05}Sc_{0.01}Cr_{0.03}Mn_{1.96}O_4$.

References

[1] D. Song, H. Ikuta, T. Uchida, M. Wakihara, Solid State Ionics 117 (1999) 151.
[2] D. Guyomard, J.M. Tarascon, J. Electrochem. Soc. 139 (1992) 937.
[3] J.M. Tarascon, W.R. Mckinnon, F. Coowar, D. Guyomand, J. Electrochem. Soc. 141 (1994) 1421.
[4] Y. Xie, Y. Xu, L. Yan, Z. Yang, R. Yang, Solid State Ionics 176 (2005) 2563–2569.
[5] G. T.-K. Fey, C.-Z. Lu, T. Prem Kumar, Mater. Chem. Phys. 80 (2003) 309–318.
[6] C. Julien, I. Ruth Mangani, S. Selladurai, M. Massot, Solid State Sci. 4 (2002) 1031–1038.
[7] K. Amine, H. Tukamoto, H. Yasuda, Y. Fujita, J. Power Sources 68 (1997) 604.
[8] J.R. Dahn, T. Zheng, C.L. Thomas, J. Electrochem. Soc. 145 (1998) 851.
[9] L. Hernan, J. Morales, L. Sanchez, J. Santos, Solid State Ionics 118 (1999) 179.
[10] S.J. Hong, S.H. Chang, C.H. Yo, Bull. Korean Chem. Soc. 20 (1999) 53.
[11] C. Sigala, A.G. Salle, Y. Piffard, D. Guyomard, J. Electrochem. Soc. 148 (2001) A819.
[12] C. Sigala, A.G. Salle, Y. Piffard, D. Guyomard, J. Electrochem. Soc. 148 (2001) A826.
[13] L. Guohua, H. Ikuta, T. Uchida, M. Wakihara, J. Electrochem. Soc. 143 (1996) 178.
[14] G.X. Wang, D.H. Bradhurst, H.K. Liu, S.X. Dou, Solid State Ionics 120 (1999) 95–101.
[15] S.T. Myung, S. Komaba, N. Kumagai, J. Electrochem. Soc. 148 (5) (2001) A482.
[16] H. Ikuta, K. Takanaka, M. Wakihara, Thermochim. Acta 414 (2004) 227–232.
[17] A. John, Dean in Lange's Handbook of Chemistry (13th ed.) 1972, Thermodynamic Properties, Table 9-1 Elements and Inorganic compounds 2005.
[18] J.M. Tarascon, E. Wang, F.K. Shokoohi, J. Electrochem. Soc. 138 (1991) 2859.